JOURNAL OF SPACECRAFT AND ROCKETS
Vol. 32, No. 2, March–April 1995

Two-Dimensional Radiative Heat-Transfer Calculations for Nonequilibrium Flows

Gregory J. Elbert*
North Carolina A&T State University, Greensboro, North Carolina 27411
and
Pasquale Cinnella†
ERC for Computational Field Simulation, Mississippi State, Mississippi 39762

The present study details the inclusion of radiative heat-transfer phenomena in the numerical simulation of reactive hypersonic and atmospheric re-entry flows. Truly two-dimensional algorithms are developed for the radiative source term in the governing equations, whereby the determination of the specific intensity field is obtained by means of a numerical integration over directions of propagation of radiation. The one-dimensional slab approximation is lifted, and the analysis presented allows the determination of the radiative characteristics of the entire flowfield, rather than being limited to the stagnation streamline, thereby providing an accurate assessment of two-dimensional relieving effects in the stagnation region. A few preliminary results are presented for the Mach 47 flow over a cylinder, including a comparison of the two-dimensional algorithm with the one-dimensional approximation and an emission-dominated case. The effects of improving the modeling of radiative heat transfer are demonstrated.

I. Introduction

IN recent years, renewed interest in the field of hypersonic aerodynamics has been registered among the scientific community. The Space Shuttle and the European Hermes are fully operational and in an advanced design stage, respectively. Other aircraft, such as the National Aerospace Plane (NASP) and the European Hypersonic Transport Vehicle, are becoming national priorities and subjects for commercial competition. The Aeroassisted Orbital Transfer Vehicle (AOTV) is being conceived as an essential tool for possible exploratory missions on Mars and for efficient satellite management in high-centered orbits.[1]

In this context, it is widely recognized that radiative heat transfer plays a major role in the thermal loads associated with high-speed flight.[2] Anderson[3] shows that at the stagnation point of a blunt body the importance of convective heat transfer becomes negligible when compared with radiative loads. For vehicles like the Galileo Probe, designed for Jovian exploration, the heating will be virtually all radiative because convective heating is hindered by massive ablation.[4] Consequently, there is a practical need for reliable simulations of radiative heat transfer, which would complement the existing capabilities for the prediction of dissociation and ionization phenomena.[5]

The mathematical and physical features of fluid flow in the presence of radiative heat transfer were already well established in the 1960s.[6] The integrodifferential equations that govern relativistic flows, and their simplified version valid for "usual" gasdynamic applications, where the light speed can be considered to be infinite, are presented by Simon.[7] Radiative pressure and radiative energy density are usually insignificant for nonrelativistic applications, and are neglected by most investigators.[8]

Approximate solutions, both analytical and numerical, have been attempted for flow problems involving some form of radiative heat transfer. Zhigulev, Romishevskii, and Vertushkin[8] present analytical results for the supersonic flow over a wedge, using a linearized form of the governing equations and neglecting radiative absorption (optically thin gas). The effect of thermal radiation on the internal structure of a shock wave was established by Heaslet and Baldwin,[9] who demonstrated the possibility of discontinuous temperature and velocity profiles even in the presence of strong radiative effects. Their analysis was based on inviscid, one-dimensional flows in chemical equilibrium, and the exponential approximation was used to transform the integrodifferential problem to a purely differential form. Also, the gray-gas hypothesis was employed, that the absorption coefficient is independent of the radiation frequency. Pearson[10] removed the exponential approximation and obtained solutions for some of the cases considered by Heaslet and Baldwin. However, his numerical technique failed to converge in a few more challenging cases. Other approximate solutions for the unsteady, one-dimensional shock waves have been obtained by Olfe,[11] in connection with a linearized approach, and by Wang,[12] in connection with a self-similar treatment.

A survey of the important effects that influence the analysis of radiating flows is given by Anderson,[3] who shows by comparison that treating a gas as transparent or gray and using an uncoupled approach can significantly affect the solutions obtained. Other factors to be considered are: the need for including atomic line as well as continuum spectra in the radiative models, the possibility of strong ablative effects,[13] the importance of nonequilibrium chemistry and thermodynamics, and the necessity of three-dimensional investigations away from the stagnation region. The influence of viscosity on the radiative flowfield is examined by Traugott.[14]

The radiative properties of air and the relevant bound-bound and bound-free transitions were investigated in the 1960s,[8] and attempts to consider the coupling of finite-rate chemistry effects (photoionization) with nonequilibrium radiation for helium and argon were successful[15] for one-dimensional problems, using simplifications in the radiative transport equation. More recently, nonequilibrium radiative properties of air, including the effects of negative ions,[16] have been studied.[17]

The state of the art in the area is summarized in a recent book by Anderson.[18] A one-dimensional space approximation, known as the 1D slab geometry, is used for numerical computations. The analysis ignores two- and three-dimensional relieving effects and is valid only in a restricted region close to the stagnation point. To this effect, it might be useful to point out that already in 1965, a study by Traugott[14] identified the one-dimensional approximation as a potential liability for aerodynamic applications of radiative heat transfer simulations. More recently, Hartung and Hassan[19] compared the 1D slab model with a modified differential approach,

Presented as Paper 92-0121 at the AIAA 30th Aerospace Sciences Meeting, Reno, NV, Jan. 6–9, 1992; received July 12, 1993; revision received June 9, 1994; accepted for publication June 9, 1994.

*Research Associate, Department of Mechanical Engineering. Member AIAA.

†Assistant Professor of Aerospace Engineering. Member AIAA.

and showed that the former is inaccurate if used away from the stagnation point. Moreover, the practical design of vehicles such as the Jovian probe[4,13] has been performed using reduced versions of the governing equations, known as the viscous-shock-layer equations, and assuming equilibrium chemistry for conditions where finite-rate chemistry is likely to play a fundamental role.[20]

In the hypersonic flow regime, radiative heat transfer will occur for conditions in which the medium is chemically active and possibly out of thermodynamic equilibrium.[17] The numerical simulation of flows in thermochemical nonequilibrium has been investigated by several scientists, and results for two- and three-dimensional geometries have been obtained either neglecting radiative heat-transfer effects[5,21,22] or post-processing the converged flowfield solution to obtain the radiative field, utilizing the 1D slab approximation[23] in what amounts to a fully uncoupled approach. It is important to reiterate that the uncoupled approach has been found to significantly overestimate the radiative and conductive heat fluxes.[3]

This study describes a practical technique for performing truly two-dimensional numerical solutions to the radiative heat-transfer equations, fully coupled with an existing thermochemical nonequilibrium flow solver.[5] The focus of the present effort is directed towards the derivation and assessment of the two-dimensional algorithm. In particular, the differences between the predictions obtained with the proposed technique and those available by using the one-dimensional and the optically-thin-gas assumptions will be considered in order to determine the usefulness of the fully two-dimensional approach. Furthermore, the computational requirements for fully coupled, two-dimensional radiative heat-transfer calculations will be determined and compared with those for the simplified approaches.

Because of the complexity and computational requirements of the present task, some simplifications have been deemed necessary in both thermochemical and radiative models utilized for these preliminary results. In particular, thermodynamic equilibrium has been assumed throughout the development of the proposed techniques, and a simple five-species air model,[5] which does not al low for ionization, has been utilized for the viscous computations. However, some inviscid results are presented that utilize an eleven-species air model, which includes positive ions and electrons.[24] Moreover, a gray-gas model has been utilized for the evaluation of radiative heat transfer, and this could be a severe hindrance to the accuracy of re-entry flow predictions.[3] However, the internal consistency of the comparisons has been maintained, because all of the results have been obtained using the same thermochemical models and absorptivity coefficients; therefore a qualitative assessment of the importance of truly two-dimensional radiative heat-transfer models can be made. It may be useful to point out that the technique proposed is by no means limited to gray gases; virtually any existing radiative model could be used to obtain more reliable quantitative predictions of radiative heat transfer.

The present approach can be extended to axisymmetric and fully three-dimensional geometries.[25] The computational requirements increase, but not dramatically. More details are given by Elbert.[26]

In the following, the mathematical and physical foundations for the study of flows in chemical nonequilibrium will be briefly outlined, including radiative heat-transfer effects. A discussion of the numerical techniques employed for the discretization of the flow equations and the determination of the source term due to the presence of a radiation field will follow. A few preliminary results will be presented in order to assess the main features of the present algorithm in comparison with simplified approaches, as well as its computational requirements.

II. Thermodynamic Model

At high temperatures, imperfect-gas effects are due to chemical changes in the amount of mass of each species and to the activation of internal energy modes that behave nonlinearly with temperature. As long as the pressure is sufficiently low, away from the gas triple point, each species of the gas mixture will behave as a thermally perfect gas. In the following, a gas mixture composed of N species will be considered. The internal energy per unit mass of species i can be defined as

$$e_i = \int_{T_{\text{ref}}}^{T} c_{vi}(\tau)\,\mathrm{d}\tau + h_{fi} \tag{1}$$

where e_i has been expressed in terms of the specific heat at constant volume, c_{vi}. In the above, T is the temperature, and h_{fi} is the heat of formation at the reference temperature T_{ref}.

The thermal equation of state for a mixture of thermally perfect gases will be given by Dalton's law, whereby the mixture pressure is the summation of partial pressures:

$$p = \sum_{i=1}^{N} \rho_i R_i T = \rho \tilde{R} T \tag{2}$$

where mass density ρ and gas constant $\tilde{R}$ for the mixture are evaluated by means of the species values ρ_i and R_i, respectively, as follows:

$$\rho = \sum_{i=1}^{N} \rho_i, \qquad \tilde{R} \equiv \sum_{i=1}^{N} \frac{\rho_i}{\rho} R_i \tag{3}$$

The state relationship of the pressure to the specific internal energy occurs implicitly through the temperature. For a given chemical composition and internal energy, the temperature must be evaluated from the caloric equation of state

$$e = \sum_{i=1}^{N} \frac{\rho_i}{\rho} \left[\int_{T_{\text{ref}}}^{T} c_{vi}(\tau)\,\mathrm{d}\tau + h_{fi} \right] \tag{4}$$

where e is the mixture internal energy, expressed in terms of the species contributions. Iterative procedures are used to solve for T. Once the temperature is found, the pressure is determined from (2).

III. Governing Equations

The governing integrodifferential equations for a reacting gas in radiative nonequilibrium, with the inclusion of relativistic effects, have been derived by Simon.[7] However, most hypersonic problems will be such that relativistic effects can be neglected,[8] which amounts to considering the speed of light to be infinite. In those cases, radiative pressure and radiant energy density will be negligible, and the only contribution from radiative nonequilibrium to the gasdynamic equations will be the inclusion of the divergence of the radiant heat flux vector. This additional term can be written as an integral involving the specific intensity of radiation I_ν, and treated as a source term for the global energy equation.

Within this nonrelativistic framework, the governing equations for a two-dimensional flow with nonequilibrium chemistry may be written in vector conservation form, using generalized coordinates, as follows:

$$\frac{\partial}{\partial t}\left(\frac{\boldsymbol{Q}}{J}\right) + \frac{\partial \tilde{\boldsymbol{F}}}{\partial \xi} + \frac{\partial(\tilde{\boldsymbol{G}} - \tilde{\boldsymbol{G}}_v)}{\partial \eta} = \frac{\boldsymbol{W}}{J} \tag{5}$$

where $\boldsymbol{Q}$ is the vector of conserved variables, $\tilde{\boldsymbol{F}}$, $\tilde{\mathbf{G}}$ are the inviscid flux vectors, $\tilde{\boldsymbol{G}}_v$ is the viscous flux vector, and $\boldsymbol{W}$ is the vector of source terms. Equation (5) represents $N + 3$ conservation equations, with the first N corresponding to species continuity, followed by the momentum and the total energy conservation equations. In the above, J is the Jacobian of the coordinate transformation between the orthogonal Cartesian frame (x, y) and the generalized curvilinear frame (ξ, η).

The vectors $\boldsymbol{Q}$ and $\boldsymbol{W}$ are given by

$$\boldsymbol{Q} = \begin{bmatrix} \rho_1 \\ \rho_2 \\ \vdots \\ \rho_N \\ \rho u \\ \rho v \\ \rho e_0 \end{bmatrix}, \qquad \boldsymbol{W} = \begin{bmatrix} w_1 \\ w_2 \\ \vdots \\ w_N \\ 0 \\ 0 \\ -\nabla \cdot \boldsymbol{q}^R \end{bmatrix} \tag{6}$$

where body forces have been neglected. In the above, $\boldsymbol{u}$ is the mass-averaged velocity vector (whose Cartesian components are u, v), and e_0 is the total energy per unit mass, $e_0 = e + (u^2 + v^2)/2$. The source terms for the species continuity equations, w_i, represent chemical production for the ith species.[5]

The component $\nabla \cdot \boldsymbol{q}^R$ is the divergence of the radiant heat flux vector, and for two-dimensional problems it is given by

$$\nabla \cdot \boldsymbol{q}^R = \int_0^\infty 2 \int_0^{2\pi} \boldsymbol{l} \cdot \nabla I_\nu \, \mathrm{d}\phi \, \mathrm{d}\nu \tag{7}$$

where ν is the frequency, $\mathrm{d}\phi$ is a differential angle lying in the plane under consideration, and I_ν is the specific intensity of radiation, or the radiant energy flux, per unit angle per unit frequency, across a surface normal to the direction of propagation of the radiation, $\boldsymbol{l}$. The angle ϕ and the unit vector $\boldsymbol{l}$ are related by the fact that $\boldsymbol{l}$ is centered at the infinitesimal angle $\mathrm{d}\phi$:

$$l_x = \cos\phi, \qquad l_y = \sqrt{1 - \cos^2\phi} = \sin\phi \tag{8}$$

Consequently, in the following the angle ϕ and the direction cosines l_x, l_y will be used interchangeably. At a given instant in time and position, I_ν is a function of the direction cosines l_x, l_y and of the frequency ν, so that $I_\nu = I_\nu(t, \xi, \eta, l_x, l_y, \nu)$. Consequently, the integration in Eq. (7) is carried over all frequencies and all angles (or directions of propagation).

Expressions for the inviscid flux vectors $\tilde{\boldsymbol{F}}, \tilde{\boldsymbol{G}}$ and the viscous flux vector $\tilde{\boldsymbol{G}}_v$, and details on the modeling of viscosity, thermal conductivity, and diffusion phenomena, are given by Walters et al.[5]

The mathematical closure to the system of integrodifferential equations (5) is provided by the density definition (3); the equation of state, defined implicitly through (2) and (4), giving the pressure in terms of conserved variables; and the equation of radiative transfer, to be discussed in the next section, providing a differential equation for the space variation of the specific intensity in terms of the gas properties.

IV. Radiative Heat Transfer

A. Equation of Radiative Transfer

The equation of radiative transfer is a continuity equation for the number of photons in the differential solid angle $\mathrm{d}\Omega$ and for the differential frequency range $\mathrm{d}\nu$. It involves chemical-reaction-type terms, which take into account emission and absorption of radiation, and it should include elastic-collision-type terms to model scattering. However, scattering is usually neglected in gasdynamic applications.[6] This equation describes the variation of specific intensity along a direction of propagation $\boldsymbol{l}$, and reads

$$\boldsymbol{l} \cdot \nabla I_\nu = \alpha_\nu [B_\nu(T) - I_\nu] \tag{9}$$

where α_ν is the volumetric absorption coefficient, and $B_\nu(T)$ is the equilibrium value of the specific intensity, given by

$$B_\nu(T) = \frac{2h\nu^3/c^2}{e^{h\nu/kT} - 1} \tag{10}$$

In the above, c is the speed of light, h is the Planck constant, and k is the Boltzmann constant. Furthermore, a simplified model for the radiative interaction was utilized, which is known as the quasiequilibrium hypothesis.[6] In brief, quasiequilibrium implies that the populations of the excited atomic states are given by their equilibrium values, controlled by collisional processes, and are not perturbed by the presence of emission and absorption. The collisional processes are also considered to be in quasiequilibrium according to a Boltzmann distribution. In general, it is a nontrivial task to obtain fully nonequilibrium models of radiative heat transfer for gas mixtures of practical interest, although some effort has been registered in the scientific community.[15–17]

The solution to the equation of radiative transfer (9) will give the specific intensity at a given angle (direction of propagation) for a given frequency. For direction $\boldsymbol{l}$, this equation can be written as follows:

$$\frac{\mathrm{d}I_\nu}{\mathrm{d}r} = -\alpha_\nu (B_\nu - I_\nu) \tag{11}$$

where the directional derivative $\mathrm{d}(*)/\mathrm{d}r = -\boldsymbol{l} \cdot \nabla(*)$ has been defined in the direction opposite to the direction of propagation of radiation. The final solution for the specific intensity reads

$$I_\nu(r) = I_\nu(\infty) \exp\left(- \int_r^{r_\infty} \alpha_\nu \, \mathrm{d}z \right) + \int_r^{r_\infty} \alpha_\nu B_\nu \exp\left(- \int_r^w \alpha_\nu \, \mathrm{d}z \right) \mathrm{d}w \tag{12}$$

where w and z are dummy variables of integration, and the boundary condition $I_\nu = I_\nu(\infty)$ at $r = r_\infty$ has been imposed. The physical meaning of the previous equation is that the specific intensity at a point r is given by the boundary value, attenuated by absorption, plus the contribution from emission of all the particles lying along the direction of propagation, again attenuated by absorption.

Substituting the equation of radiative transfer (9) into the expression (7) for the divergence of the radiant heat flux vector yields

$$\nabla \cdot \boldsymbol{q}^R = \int_0^\infty \alpha_\nu \left(4\pi B_\nu - 2 \int_0^{2\pi} I_\nu \, \mathrm{d}\phi \right) \mathrm{d}\nu \tag{13}$$

The complete determination of the radiative source term in the governing equations (5) is obtained, for this approximate quasiequilibrium case, when the integrals in (12) are evaluated at the given point in space and time to yield a value of the specific intensity for a given direction of propagation. The procedure is then repeated for all directions and for all radiative frequencies in order to determine the value of the divergence of the radiative heat flux vector, Eq. (13).

B. Radiative Source Term

As previously stated, the presence of a radiation field manifests itself in the governing fluid-dynamic equations (5) as a source term, of the kind described in Eq. (13) if the quasiequilibrium hypothesis is utilized. The peculiar character of this source term is that it is not local, but its determination requires the knowledge of the thermophysical and radiative properties of the flowfield in a global fashion. More specifically, for every point in space, described by the coordinates (ξ, η), and at a given time t, it is possible to define a local cylindrical coordinate system (r, ϕ) centered at the point under consideration. Then the specific intensity at the point is given by Eq. (12) with $r = 0$. It might be useful to repeat that the specific intensity is a function of time, position, direction of propagation, and frequency: $I_\nu = I_\nu(t, \xi, \eta, \phi, \nu)$. The expression (12) is valid for a given direction of propagation, described by the angle ϕ, and for a given frequency, and its form shows that the result depends upon the thermophysical and radiative properties of all the points along the direction of propagation, that is, all the points along a ray that originates at the boundary r_∞ and reaches the point under consideration at $r = 0$. Typical boundary points will be the far-field and solid boundaries.

Substitution of the expression (12) or the specific intensity into the divergence (13) of the radiant heat flux vector yields

$$\nabla \cdot \boldsymbol{q}^R = 4\sigma\alpha_P T^4 - 2 \int_0^\infty \alpha_\nu \left[\int_0^{2\pi} I_\nu(\infty) \times \exp\left(- \int_0^{r_\infty} \alpha_\nu \, \mathrm{d}z \right) \mathrm{d}\phi \right] \mathrm{d}\nu - 2 \int_0^\infty \alpha_\nu \left[\int_0^{2\pi} \int_0^{r_\infty} \alpha_\nu B_\nu \times \exp\left(- \int_0^w \alpha_\nu \, \mathrm{d}z \right) \mathrm{d}w \, \mathrm{d}\phi \right] \mathrm{d}\nu \tag{14}$$

where the Planck mean absorption coefficient α_P has been introduced:

$$\alpha_P \equiv \frac{\int_0^\infty \alpha_\nu B_\nu \, \mathrm{d}\nu}{\int_0^\infty B_\nu \, \mathrm{d}\nu} = \frac{\pi}{\sigma T^4} \int_0^\infty \alpha_\nu B_\nu \, \mathrm{d}\nu \tag{15}$$

and σ is the Stefan-Boltzmann constant. It is apparent from this form of the radiative source term that its value at any point in the flowfield at a given time will depend upon the properties of all the points that are in its "line of sight," that is, all the points lying in the portion of the flowfield that is swept by straight lines (rays) emanating from the point under consideration and terminating either at solid boundaries or in the far field.

The expression for the divergence of the radiant heat flux vector, Eq. (14), is complicated and difficult to evaluate numerically. In order to simplify its treatment, the 1D slab approximation has been introduced and is almost universally adopted in practical calculations.[18] In summary, the approximation consists in neglecting two-dimensional (and three-dimensional) effects in the vicinity of the stagnation streamline, reducing the shock-layer region around a blunt body to a slab whose physical properties vary in one dimension only.[6] Consequently, the integration over the direction of propagation is considerably simplified, and the final expression for the divergence of the radiant heat flux vector reads

$$\nabla \cdot \boldsymbol{q}^R = 4\sigma\alpha_P T^4 - 2\pi \int_0^\infty \alpha_\nu \left[I_\nu(-\infty) E_2\left(-\eta^\nu_{-\infty}\right) + I_\nu(+\infty) E_2\left(+\eta^\nu_{+\infty}\right)\right] d\nu - 2\pi \int_0^\infty \alpha_\nu \left[\int_{-\infty}^0 \alpha_\nu B_\nu E_1(-\eta^\nu)\, dx + \int_0^{+\infty} \alpha_\nu B_\nu E_1(\eta^\nu)\, dx \right] d\nu \tag{16}$$

where E_i is the integroexponential function of order i, and η^ν is the optical thickness of the gas:

$$E_i(z) = \int_0^1 w^{i-2} e^{-z/w}\, dw, \qquad \eta^\nu = \int_0^x \alpha_\nu\, dx. \tag{17}$$

In the above, the integration over the direction of propagation ϕ has been simplified and is taken into account by the presence of the integroexponential function. The radius x originates at one boundary point ($-\infty$, e.g., the freestream) and ends at the other boundary point ($+\infty$, e.g., the body), going through the slab and passing through the location of the finite volume under consideration (point 0). The direction x is the local normal direction to the body. In the derivation of the 1D slab approximation, it is assumed that the flow properties vary only in the direction perpendicular to the slab (i.e., from the freestream to the body). It is apparent that this assumption will be reasonable only in a small region close to the stagnation streamline, because the changes in the flowfield in the direction tangential to the body are far from being negligible in general.

In some cases, an even more drastic simplification is made to the modeling of the radiative source term, namely, the emission-dominated approximation.[6] This provides a simple expression for the divergence of the radiant heat flux vector,

$$\nabla \cdot \boldsymbol{q}^R = 4\sigma\alpha_P T^4 \tag{18}$$

which is a local contribution only, and does not depend upon directions of propagations and/or lines of sight. A condition for a gas to be emission-dominated is that its optical thickness η^ν must be small for the entire frequency range, which is a reasonable assumption for some practical problems, but not very accurate in general.[3]

C. Radiative Heat Flux Vector

In practical applications, it is necessary to know or at least estimate the aerothermodynamic heating associated with a given hypersonic flight condition. Consequently, the radiative heat flux vector $\boldsymbol{q}^R$ itself needs be determined, not just its divergence as in the previous section.

For a two-dimensional problem, the vector $\boldsymbol{q}^R$ is defined as

$$\boldsymbol{q}^R = 2\int_0^\infty \int_0^{2\pi} I\boldsymbol{I}_\nu\, d\phi\, d\nu \tag{19}$$

Introducing a unit vector $\boldsymbol{r} = -\boldsymbol{l}$, oriented in the direction opposite to the direction of propagation of radiation, and substituting Eq. (12) into Eq. (19) yields

$$\boldsymbol{q}^R = -2\int_0^\infty \left[\int_0^{2\pi} I_\nu(\infty)\boldsymbol{r} \exp\left(-\int_0^{r_\infty} dz \right) d\phi \right] d\nu - 2\int_0^\infty \left[\int_0^{2\pi} \int_0^{r_\infty} \alpha_\nu B_\nu \boldsymbol{r} \exp\left(-\int_0^w \alpha_\nu\, dz \right) dw\, d\phi \right] d\nu \tag{20}$$

It is important to point out that the determination of $\boldsymbol{q}^R$ requires evaluating the same kind of integrals that were encountered in the definition of its divergence, as seen in Eq. (14).

When the 1D slab approximation is used, the only nonzero component of the heat flux vector is the one in the main direction of propagation of radiation, normal to the body. The final results reads

$$q_x^R = -2\pi \int_0^\infty \left[I_\nu(+\infty) E_3\left(+\eta^\nu_{+\infty}\right) - I_\nu(-\infty) \times E_3\left(-\eta^\nu_{-\infty}\right)\right] d\nu - 2\pi \int_0^\infty \left[\int_0^{+\infty} \alpha_\nu B_\nu E_2(\eta^\nu)\, dx - \int_{-\infty}^0 \alpha_\nu B_\nu E_2(-\eta^\nu)\, dx \right] d\nu \tag{21}$$

Again, only integrations along the main direction of propagation and for the frequency spectrum are necessary.

Considering the emission-dominated case, and utilizing the quasi-one-dimensional geometric framework, it can be verified that the radiative heat flux vector in the main direction of propagation is given by the limiting case of Eq. (21) for the optical thickness η^ν going to zero (optically thin gas). Consequently, the integroexponential functions reduce to

$$E_3(0) = \tfrac{1}{2}, \qquad E_2(0) = 1 \tag{22}$$

and the final result reads

$$q_x^R = -\pi \int_0^\infty [I_\nu(+\infty) - I_\nu(-\infty)]\, d\nu - 2\pi \int_0^\infty \left[\int_0^{+\infty} \alpha_\nu B_\nu\, dx - \int_{-\infty}^0 \alpha_\nu B_\nu\, dx \right] d\nu \tag{23}$$

V. Numerical Formulation

A. Governing Equations

The governing partial differential equations for hypersonic flows out of chemical equilibrium that have been presented in Sec. III are discretized using the finite-volume technique,[27] whereby their integral form is solved for the unknown volume averages of conserved variables in some small, but finite, control volume. The integral form reads

$$\int\int_{\mathcal{V}} \frac{\partial \boldsymbol{Q}}{\partial t}\, d\mathcal{V} + \oint_{\mathcal{S}} (\boldsymbol{S} - \boldsymbol{S}_v) \cdot \boldsymbol{n}\, d\mathcal{S} = \int\int_{\mathcal{V}} \boldsymbol{W}\, d\mathcal{V} \tag{24}$$

where $\mathcal{V}$ is an arbitrary volume closed by a boundary $\mathcal{S}$, and $\boldsymbol{S}$, $\boldsymbol{S}_v$ are inviscid and viscous flux vectors, respectively, evaluated at the boundary. Approximations are then used for the volume and surface integrals to express them in terms of the unknown volume-averaged values for each computational cell. The discretization of the inviscid fluxes is accomplished by means of flux-split techniques, and a thorough derivation of the algorithms can be found in Grossman and Cinnella.[28] Central differences are used for the viscous fluxes.

The discretized equations are advanced in time using either an *LU* decomposition or an approximate factorization. More details are given in Walters et al.[5]

B. Radiative Source Term and Flux Vector

The numerical evaluation of the radiative source terms (14) involves integration over frequency, over angle, and over length along a direction of propagation. This evaluation should be performed at every time step when time accuracy is of interest. However, for steady-state problems, the radiative source terms can be lagged for a few time steps. It might be useful to point out that the "ultimate" lagging, that is, the evaluation of the source terms at convergence only, is tantamount to a fully decoupled approach, which is the strategy employed by Candler and Park[23] in conjunction with the one-dimensional approximation.

The integration over the frequency spectrum can be performed in its simplest form by means of the gray-gas approximation.[6] More realistic approaches include the three-band and the eight-band model,[3] whereby the mean absorption coefficient is considered constant over a frequency band, and the integration reduces to a summation over the bands. The present study has utilized the one-band (gray-gas) model only for simplicity, although provisions for multiple-band models were included.

The double integration over the geometric parameters (angle and length) is accomplished by superimposing a "radiation grid" on the discretized domain. In particular, for every finite volume in the calculation it is necessary to define the rays that will be considered for the integration over the angle, and the points along each ray for the integration over the length, including the boundary points in the far field or at some solid wall. Specifically, given a computational cell and a direction of propagation, a ray is started from the cell center and continued until a boundary is reached. After locating the boundary point at the intersection of the ray with the grid boundary, the points along the ray are distributed in accordance with the technique chosen for the line integration. The process is continued until all directions of propagation are exhausted, and is repeated for all volumes in the computational domain.

The integration over the angle (direction of propagation) is performed by partitioning the interval $[0, 2\pi]$ into equally distributed subintervals. Because the two limits of integration physically coincide, this procedure is tantamount to using a composite trapezoidal rule (or a two-point open Newton-Cotes formula). Several options have been implemented for the integration over the length, including composite trapezoidal and Simpson rules, the use of Richardson's extrapolation, and the implementation of a composite Gauss-Legendre formula.

In order to be able to follow a ray until a boundary is reached, it becomes necessary to determine to which cell a given point on the ray belongs. Moreover, once the distribution of points along a ray is found, the numerical integration procedure requires the knowledge of the value of the integrand at each point. The simplest way of evaluating the integrand is to assume that the thermophysical and radiative properties of a point under consideration are the same as those of the cell that contains it. In both cases it is vital to determine the computational cell that contains a given point in physical space. A simple way of doing this is illustrated in Fig. 1. Point 0 is the point under consideration, and a trial cell has been selected, whose corners are numbered from 1 to 4 in a counterclockwise fashion. Defining $\boldsymbol{R}_{ij}$ as the vector from point i to point j, four cross products are calculated, as follows:

$$\begin{aligned} A_{012}\boldsymbol{k} &= \boldsymbol{R}_{01} \times \boldsymbol{R}_{12} \\ A_{023}\boldsymbol{k} &= \boldsymbol{R}_{02} \times \boldsymbol{R}_{23} \\ A_{034}\boldsymbol{k} &= \boldsymbol{R}_{03} \times \boldsymbol{R}_{34} \\ A_{041}\boldsymbol{k} &= \boldsymbol{R}_{04} \times \boldsymbol{R}_{41} \end{aligned} \tag{25}$$

where $\boldsymbol{k}$ is the unit vector perpendicular to the Cartesian (x, y) plane. If all four quantities A_{0ij} are positive, it is possible to show that point 0 is inside the trial cell, as shown in Fig. 2. If one or two of those quantities are negative, their signs will allow the selection of a new trial cell. In particular, if (j, k) are the indices corresponding

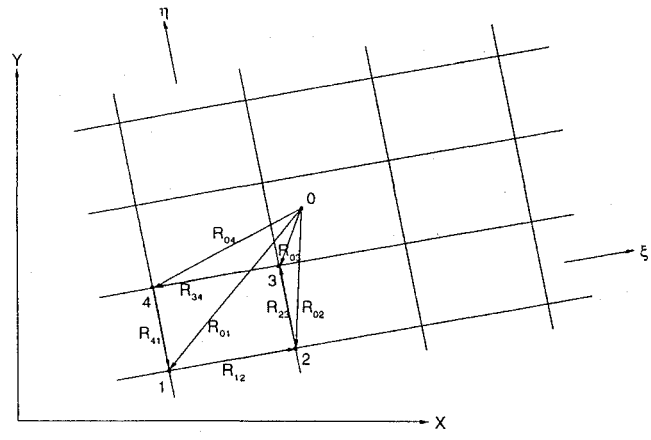

Fig. 1 Determination of the computational cell (1234) that contains point 0.

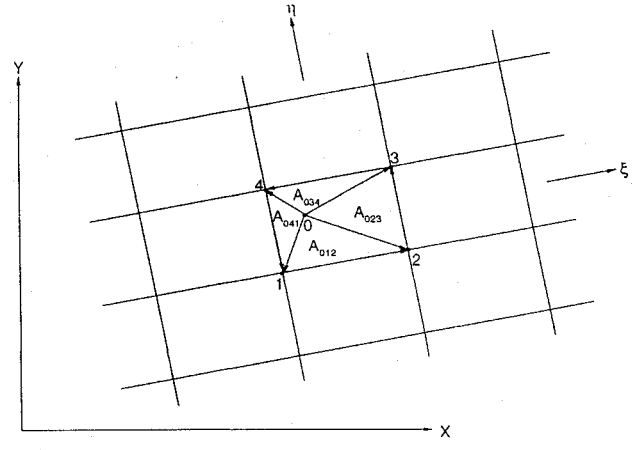

Fig. 2 All cross products are positive: point 0 is inside the cell (1234).

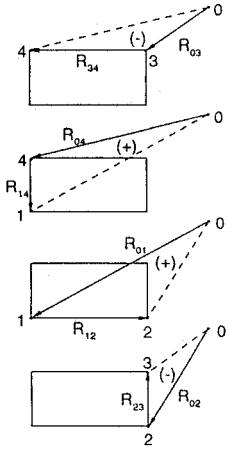

Fig. 3 A_{023} and A_{034} are negative: point 0 is to the right of and above the cell (1234).

to the trial cell in the computational domain, the indices for the new cell will be given by the following logic:

$$\begin{aligned} &\text{if} \quad (A_{023} < 0 \text{ and } A_{041} > 0) \quad \text{then} \quad j \to j+1 \\ &\text{if} \quad (A_{023} > 0 \text{ and } A_{041} < 0) \quad \text{then} \quad j \to j-1 \\ &\text{if} \quad (A_{012} > 0 \text{ and } A_{034} < 0) \quad \text{then} \quad k \to k+1 \\ &\text{if} \quad (A_{012} < 0 \text{ and } A_{034} > 0) \quad \text{then} \quad k \to k-1 \end{aligned} \tag{26}$$

An example of this case is given in Fig. 3. Because of the incremental nature of the cell update, a good initial guess for the trial cell is essential for the overall efficiency of the algorithm. Typically, the coordinates of a previously located point on a ray serve

as an excellent initial guess for the following point, and the overall procedure is quite efficient.

The determination of the radiative heat flux vector q^R follows the same steps outlined for the evaluation of the radiative source terms, since the necessary integrations are quite similar.

VI. Numerical Results

Preliminary results were obtained for a Mach 46.8 flow over a circular cylinder in air at an altitude of 57.9 km. The cylinder radius was 1.524 m, the freestream temperature was $T_\infty = 262.9$ K, the density was $\rho_\infty = 4.26 \times 10^{-4}$ kg/m^3, and the pressure was $\rho_\infty = 32.2$ N/m^2. This problem was studied by Howe and Viegas[2] by means of a shock-layer solution in equilibrium air using the 1D slab approximation. It should be reiterated that their methodology provides a prediction of the stagnation streamline variables only.

Figure 4 shows a symbolic representation of the physical grid and, superimposed on it, the "radiative grid" for a single finite volume. It should be noted that at the symmetry plane the lines of sight are specularly reflected, allowing the calculations to be performed with a quarter circumference only.

Fairly standard boundary conditions were imposed for the freestream (Dirichlet), the exit plane (extrapolation), and the stagnation streamline (tangency). At the solid wall, the viscous cases used the no-slip condition with the wall temperature fixed at 1500 K. For the inviscid cases, a special boundary condition was employed, featuring tangency, zero gradients for mass fractions and pressure, and a fixed wall temperature of 1500 K. It might be useful to point out that owing to the lack of a thermal boundary layer, the cold wall affects the solution only through its effect on the radiative source term.

Results were obtained for the truly two-dimensional radiative heat-transfer case, the 1D slab approximation, the emission-dominated case, and a baseline case with no radiative heat transfer. A Van Leer-type discretization of the inviscid fluxes was employed.[28] Unfortunately, only simulations that are first-order accurate in space were obtained, because of severe convergence problems encountered at this extremely high Mach number. A vibrational equilibrium thermodynamic model was employed for the description of the species internal energy.[5]

A. Five Species, Viscous Results

The viscous investigations employed a 61×91 grid, which corresponded to 60 volumes in the circumferential direction and 90 in the radial direction. The grid was slightly clustered near the stagnation region, and yielded Reynolds numbers based on cell width ranging from 2 at the stagnation point to about 12 at the shoulder. The Reynolds number based on the cylinder radius was 0.59×10^6, which is less than the estimated 10^8 necessary to induce transition.[18] Consequently, the flow was considered to be laminar. The radiation grid at every volume consisted of 36 equally spaced rays and 40 intervals of integration per ray, slightly clustered near the originating cell, resulting in 80 radiation-grid points along each ray. The composite two-point Gauss-Legendre formula was used for the numerical quadrature along a ray.

For these calculations, the gray-gas model for the absorption coefficient in equilibrium air given by Wang[12] was employed in conjunction with a simple five-species air model,[5] which takes account of dissociation and the formation of NO.

The temperature profiles along the stagnation streamline are shown in Fig. 5. It may be noticed that shock location and temperature values are affected by the choice of the radiative transfer model. In particular, absorption is reheating the gas in the shock layer in comparison with the emission-dominated case, but the fully two-dimensional algorithm provides the flowfield with some "relieving" effects, which ultimately result in lower temperatures than in the 1D slab approximation. The baseline case with no radiation is not presented, because it would be outside of the plotted scale on account of the dramatic (and nonphysical) increase in temperature levels for a gas that is not allowed to radiate off most of the aerothermodynamic heating associated with a Mach 47 flow.

The density values along the stagnation streamline are represented in Fig. 6, and show that radiative cooling is responsible for the dramatic density increase in the shock layer over that in the nonradiative case, even outside the boundary layer. The total enthalpy along the stagnation streamline is plotted in Fig. 7, along with the results of Howe and Viegas.[2] The quantitative discrepancy between the present calculations and those of

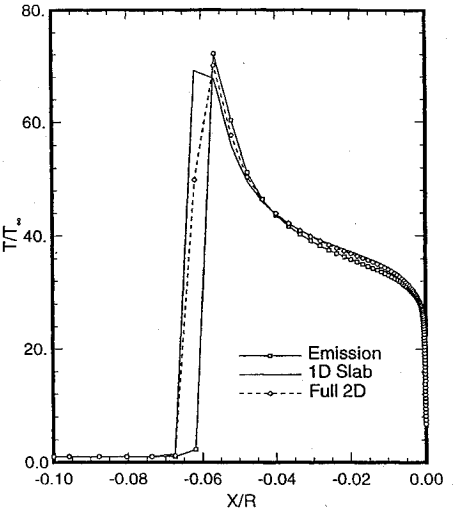

Fig. 5 Temperature along the stagnation streamline. Five species, viscous.

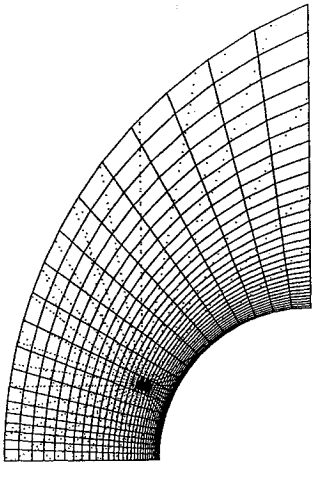

Fig. 4 Symbolic representation of the grid, showing the points used for the double integration.

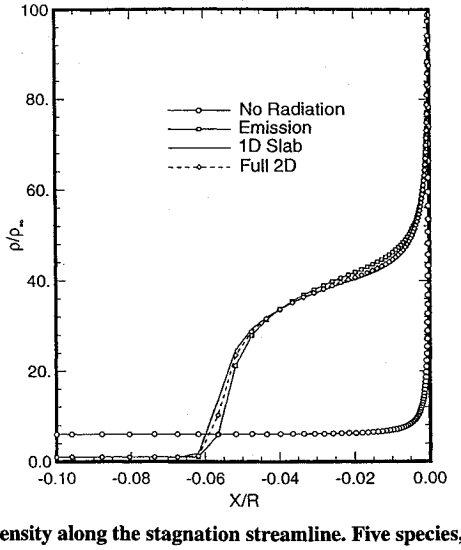

Fig. 6 Density along the stagnation streamline. Five species, viscous.

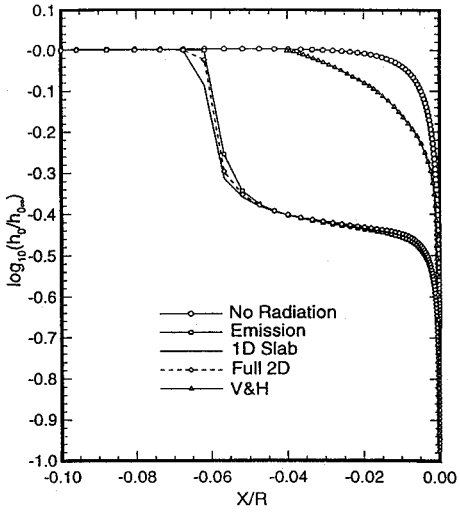

Fig. 7 Total enthalpy along the stagnation streamline. Five species, viscous.

Table 1 CPU time requirements for different radiative models

Radiation model	Time, s/iter.	
	No reuse	Reuse = 10
None	1.1599	0.5491
Emission		
1 band	1.1620	0.5533
2 band	1.1621	0.5544
4 band	1.1641	0.5556
8 band	1.1672	0.5593
1D slab		
1 band	1.4660	0.8553
2 band	1.6262	1.0157
4 band	1.9481	1.3361
8 band	2.5892	1.9787
Fully two-dimensional		
1 band	4.39	3.78
2 band	7.51	6.90
4 band	13.76	13.16
8 band	26.26	25.63

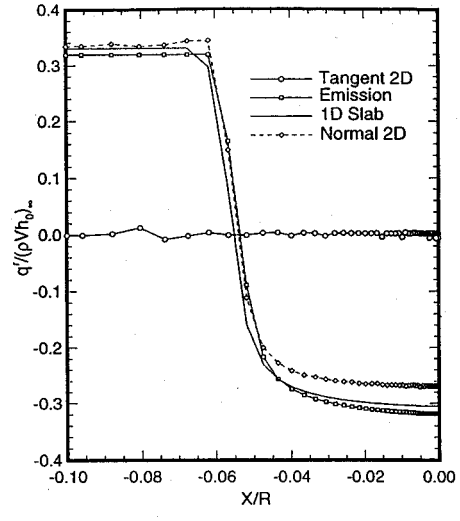

Fig. 8 Radiative heat flux along the stagnation streamline. Five species, viscous.

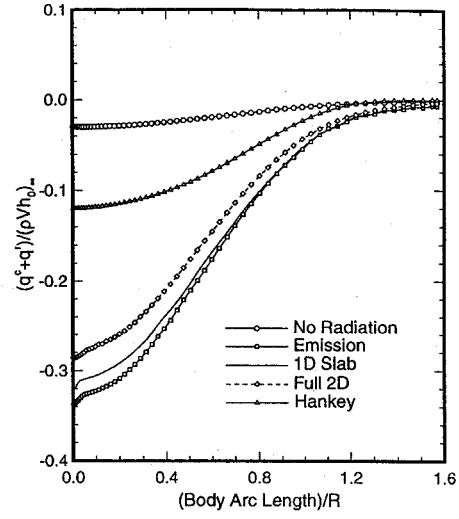

Fig. 9 Total heat flux along the body. Five species, viscous.

the previous reference is probably due to the fact that the proposed methodology captures the high-temperature gas cap at the shock, where a significant amount of energy is removed from the flow through emission. In contrast, Howe and Viegas utilize a shooting technique that asymptotically approaches the equilibrium shock jump conditions, thereby disallowing a high-temperature gas cap.

The skin friction and conduction heat-transfer coefficients along the body, not shown here, display minor differences between the different radiative models, but significantly smaller values than in the nonradiative case, by up to 26 and 44%, respectively.

The components of the heat flux vector normal to the body in the first row of volumes off the stagnation streamline are represented in Fig. 8. Also shown is the tangential component of the radiative heat flux vector for the two-dimensional case. There is a significant difference between two-dimensional and 1D slab results, although the stagnation region is the place where the one-dimensional approximation should perform best. More specifically, the radiative heat flux vector at the stagnation point has a dimensional value of 234 MW/m^2 when evaluated with the 1D slab theory, and a value of 212 MW/m^2 when calculated by means of the fully two-dimensional algorithm. The difference is about 10%.

The heat loads for these calculations are shown in Fig. 9, which depicts the component of the *total* heat flux vector normal to the body on the first row of volumes off of the body. There is a significant change between the two-dimensional and the one-dimensional predictions. It should be pointed out that the radiative heat flux is one order of magnitude larger than the conductive component, and maintains that dominance over the entire arc length, which confirms the fact that at this extreme Mach number the heating load is essentially due to radiation. Howe and Viegas's prediction at the stagnation point has been coupled with an empirical relation for the distribution of the radiative heat flux along the body, due to Hankey.[29] The trend is similar to the present result, and the quantitative disagreement is due to the differences in thermochemical models and the absence of the high-temperature gas cap in the previous reference, as already mentioned.

B. CPU Requirements

The relative computational efficiency of the different radiative models in the context of a reactive flow calculation was investigated. Table 1 shows a comparison of CPU time per iteration on a Cray Y-MP for the reactive case with no radiation, the emission-dominated problem, the 1D slab, and the full two-dimensional algorithm. The number of CPU seconds per iteration is based on timing 100 consecutive iterations. The "Reuse" column refers to the fact that the left-hand side of the approximate factorization may be selectively frozen for an arbitrary number of cycles after a minimum residual reduction is achieved. The table was prepared by implementing the freezing option after a residual reduction of two orders of magnitude and re-evaluating the left-hand side every 10 iterations. The saving in CPU time per iteration is apparent from the table. In order to study the effect of multiple-band models on the numerical

requirements, the timing runs include the simulation of one-, two-, four-, and eight-band models, obtained by breaking the frequency interval in several pieces.

Comparing the overheads associated with the inclusion of a radiative model with the baseline time for a reactive calculation, it is possible to conclude that the cost of running an emission-dominated model is negligible. On the other hand, a non-negligible increase in CPU time is required for the 1D slab calculation, especially for the eight-band model. The fully two-dimensional algorithm is considerably more expensive, leading to almost a threefold increase in CPU time without freezing and a sixfold increase with freezing for the one-band model, and requiring a full order of magnitude more time for the eight-band model. This should not be surprising in view of the fact that the evaluation of the radiative source term involves 36 rays per finite volume, instead of two as in the 1D slab.

The typical convergence strategy employed for the present work involved obtaining a solution for the emission-dominated model, then utilizing that solution as an initial guess for the 1D slab calculations, and finally using the 1D slab results as an initial guess for the fully two-dimensional predictions. However, in a preliminary stage of this study[30] the numbers of iterations required for convergence of the various radiative models perse were estimated, and found not to differ significantly. This fact means that the data just presented on CPU requirements per iteration are actually representative of the overall CPU requirements for a calculation involving one of the radiative models.

C. Grid Convergence Studies

The sensitivity of the numerical simulations to the size of the radiation grids was investigated in some detail, in order to gain more insight into the appropriate matching between flowfield and radiative source-term discretizations. In view of the low cell Reynolds numbers employed for the viscous calculations, the size of the flowfield grid was left unchanged at 61×91.

Results were obtained for several radiation-grid sizes: 36 rays and 80 points (the baseline case), 36 rays and 160 points, 72 rays and 80 points. In all cases, there was virtually no difference in the flowfield predictions (the largest differences in the temperature field were of the order of a fraction of a Kelvin, for example). This seems to confirm the fact that the original discretization of the radiative source term was sufficiently accurate.

A similar study was conducted for the discretization involved in evaluating the radiative heat flux vector itself. As already pointed out, the integrals to be evaluated are close to those used for the determination of the source term in the governing equations, and the numerical evaluation requires the use of radiation grids that are based on the same principles as those used for the source terms. The main difference is probably that the evaluation of $\boldsymbol{q}^R$ is a postprocessing operation, which is performed only once at the end of the calculations or whenever necessary for diagnostic purposes, but does not affect the evolution of the numerical solution.

The most "natural" choice for the grid size to be used for $\boldsymbol{q}^R$ would be the one used for the radiative source term, that is, 36 rays and 80 points. However, this grid gives rise to some oscillatory predictions, as shown in Figs. 10 and 11 for the heat flux along the stagnation streamline and the body, respectively. This oscillatory behavior can be corrected by refining the radiation grid, as shown in the same pictures, where a mesh of 180 rays and 500 points was employed. Because the $\boldsymbol{q}^R$ evaluation is nonrepetitive, the additional expense associated with refining the grid does not create an excessive computational burden.

D. Eleven Species, Inviscid Results

Some inviscid results were obtained on a 41×61 grid, corresponding to 40 volumes in the circumferential direction and 60 in the radial direction, slightly clustered near the stagnation region and the body surface. The radiation grid at every volume consisted of 36 equally spaced rays and 25 intervals of integration per ray, slightly clustered near the originating cell, resulting in 50 radiation-grid points along each ray. The composite two-point Gauss-Legendre formula

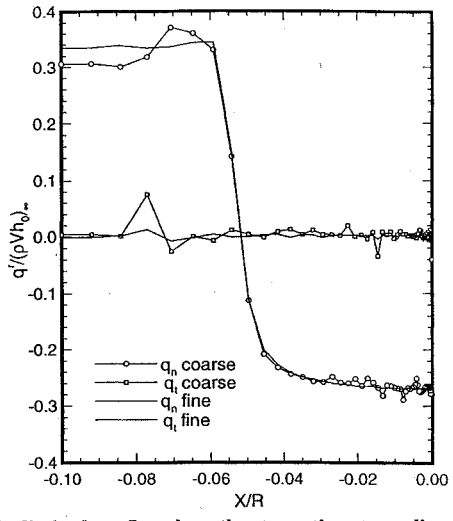

Fig. 10 Radiative heat flux along the stagnation streamline. Grid convergence study.

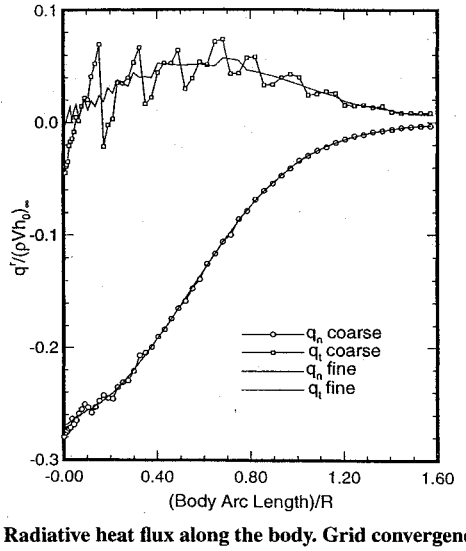

Fig. 11 Radiative heat flux along the body. Grid convergence study.

was used for the numerical quadrature along a ray. An 11-species air model due to Park[24] was employed, which includes ionization reactions, positive ions, and electrons.

For these calculations, two different absorptivity models were used and compared: the previously used model due to Wang,[12] which will be referred to as the α_1 solution, and a second model due to Viegas and Howe,[31] which will be referred to as the α_2 solution.

The purpose of these simulations is essentially twofold: investigate the presence, magnitude, and importance of ionization; and obtain at least a qualitative description of the sensitivity of the solutions to different models for absorption. Concerning the latter, it was found that the absorption coefficient in the α_2 solutions is stronger than that in the α_1 solutions. Consequently, the α_2 solutions display lower temperatures, lower stagnation enthalpy, lower degrees of dissociation and ionization, higher densities, smaller shock standoff distances, and higher radiative heat fluxes.

The solutions shown were obtained by means of the emission-dominated model for the radiative heat transfer. These solutions were postprocessed with all three radiative models in order to obtain the values of the heat flux vectors. This approach was employed for its simplicity and low computational cost, and is at least partially justified by the fact that the differences in the flowfields due to the use of the different radiative models were previously found to be minor, as long as a radiative source term was present in the governing equations.

The temperature profiles along the stagnation streamline for the two solutions are shown in Fig. 12, and detail the differences in shock

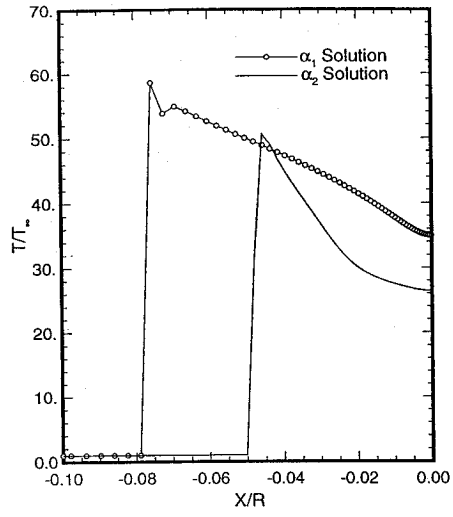

Fig. 12 Temperature along the stagnation streamline. Eleven species, inviscid.

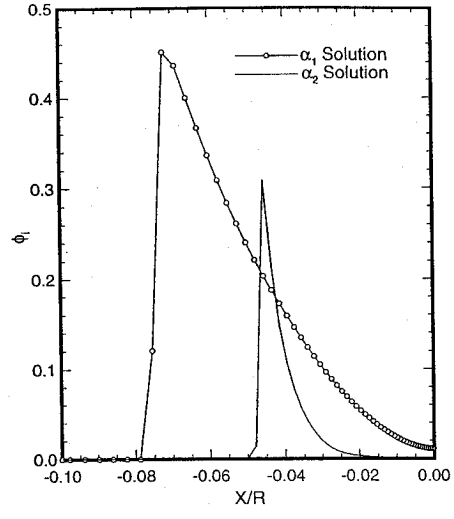

Fig. 13 Degree of ionization along the stagnation streamline. Eleven species, inviscid.

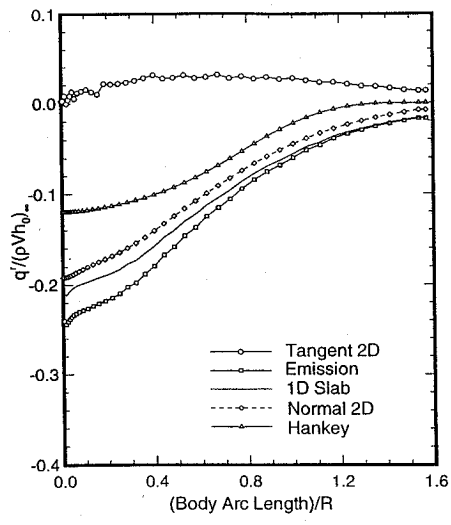

Fig. 14 Radiative heat flux along the body. Eleven species, inviscid, α_1 solution.

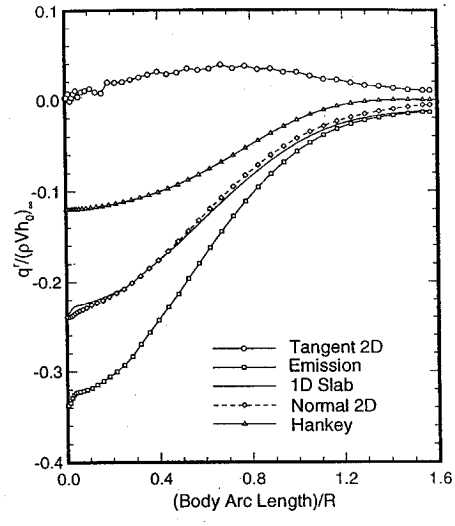

Fig. 15 Radiative heat flux along the body. Eleven species, inviscid, α_2 solution.

standoff distance and peak temperatures. A plot of the degree of ionization ϕ_l along the stagnation streamline is presented in Fig. 13. In this work, the degree of ionization is defined as the sum of the mass fractions of the ionized species. It is possible to see from the figure that the α_1 solution is much more affected by ionization than the α_2.

The heat flux along the body surface is shown in Figs. 14 and 15 for the α_1 and α_2 solutions, respectively. The α_1 solution predicts stagnation-point heating loads ranging from 144 MW/m^2 for the full two-dimensional algorithm to 181 MW/m^2 for the emission-dominated case with the quasi-one-dimensional approximation at 159 MW/m^2. The α_2 solution predicts heating loads equaling 180 MW/m^2 for both full two-dimensional and 1D slab approaches, whereas the value in the emission-dominated case is much larger, namely 250 MW/m^2. The heat load predicted by Viegas and Howe is in closer agreement with the α_1 solution.

In summary, there are some differences between the one-dimensional predictions and those obtained with the full two-dimensional model. Most notable is that the one-dimensional predictions are about 10% larger than those obtained with the two-dimensional model, when using the absorptivity coefficient due to Wang.[12] Moreover, changing the modeling of absorption is shown to have a dramatic effect on the flowfield predictions and the levels and importance of ionization. Consequently, more accurate and reliable models for the radiative properties of air are necessary for a better quantitative prediction of radiative loads.

VII. Concluding Remarks

This study is essentially based upon one idea, namely, that the one-dimensional approximation is a potential liability for the accurate determination of radiative heat transfer in problems and configurations of practical interest. The advent of modern supercomputers allows the scientist to lift this approximation, thereby making possible a thorough investigation of two-dimensional effects on thermal loads, especially when radiation is predominant. The preliminary results presented indicate that this study is warranted, practical, and useful for the achievement of improved accuracy in the simulation of radiative heat transfer. The gray-gas approximation is by no means sufficient for quantitative predictions of thermal loads in the hypersonic regime, but the techniques developed in this study are fully applicable to more refined and realistic multiband models.

Work is currently under way on axisymmetric and three-dimensional problems, with the intent of studying the feasibility of accurate radiative heat-transfer calculations for more realistic geometries.

Acknowledgments

This work was funded in part by Mississippi State University, under a Research Initiation Program sponsored by the Office of Research, and in part by the National Science Foundation, which funds the Engineering Research Center for Computational Field Simulation.

The numerical simulations presented were performed by means of an early version of the GASP code, developed principally by R. W. Walters of Virginia Polytechnic Institute and State University in Blacksburg, Virginia.

Computing time was provided by the Waterways Experiment Station in Vicksburg, Mississippi, and by the North Carolina Supercomputing Center in Research Triangle Park, North Carolina.

References

[1]Lee, J.-H., *Basic Governing Equations for the Flight Regimes of Aeroassisted Orbital Transfer Vehicles*, Vol. 96, Progress in Astronautics and Aeronautics, AIAA, New York, 1984.

[2]Howe, J. T., and Viegas, J. R., "Solution of the Ionized Radiating Shock Layer, Including Reabsorption and Foreign Species Effects, and Stagnation Region Heat Transfer," NASA TR-159, 1963.

[3]Anderson, J. D., Jr., "An Engineering Survey of Radiating Shock Layers," *AIAA Journal,* Vol. 7, No. 9, 1969.

[4]Moss, J. N., and Simmonds, A. L., *Galileo Probe Forebody Flowfield Predictions*, Vol. 85, Progress in Astronautics and Aeronautics, AIAA, New York, 1983.

[5]Walters, R. W., Cinnella, P., Slack, D. C., and Halt, D., "Characteristic-Based Algorithms for Flows in Thermo-chemical Nonequilibrium," *AIAA Journal,* Vol. 30, No. 5, 1992.

[6]Vincenti, W. C., and Kruger, C. H., Jr., *Introduction to Physical Gas Dynamics,* Krieger, Malabar, FL, 1986.

[7]Simon, R., "The Conservation Equations of a Classical Plasma in the Presence of Radiation," *Journal of Quantum Spectroscopy and Radiative Transfer*, Vol. 3, 1963.

[8]Zhigulev, V. N., Romishevskii, Y. A., and Vertushkin, V. K., "Role of Radiation in Modern Gasdynamics," *AIAA Journal*, Vol. 1, No. 6, 1963.

[9]Heaslet, M. A., and Baldwin, B. S., "Predictions of the Structure of Radiation-Resisted Shock Waves," *The Physics of Fluids,* Vol. 6, No. 6, 1963.

[10]Pearson, W. E., "On the Direct Solution of the Governing Equations for Radiation-Resisted Shock Waves," NASA TN D-2128, 1964.

[11]Olfe, D. B., "The Influence of Radiant-Energy Transfer on One-Dimensional Shock Wave Propagation," *Supersonic Flow, Chemical Processes and Radiative Transfer,* edited by D. B. Olfe and V. Zakkay, Macmillan, 1964.

[12]Wang, K. C., "The 'piston problem' with thermal radiation," *Journal of Fluid Mechanics,* Vol. 20, Pt. 3, 1964.

[13]Gupta, R., Lee, K., Moss, J., and Sutton, K., "Viscous-Shock-Layer Solutions with Coupled Radiation and Ablation Injection for Earth Entry," AIAA Paper 90-1697, 1990.

[14]Traugott, S. C., "Shock Structure in a Radiating, Heat Conducting, and Viscous Gas," *The Physics of Fluids,* Vol. 8, No. 5, 1965.

[15]Ferrari, C., and Clarke, J. H., "On Photoionization Ahead of a Strong Shock Wave," *Supersonic Flow, Chemical Processes and Radiative Transfer,* edited by D. B. Olfe and V. Zakkay, Macmillan, 1964.

[16]Soon, W. H., and Kunc, J. A., "Negative Ion Radiation in Partially Ionized Gas," AIAA Paper 90-1612, 1990.

[17]Park, C., *Calculation of Nonequilibrium Radiation in the Flight Regimes of Aeroassisted Orbital Transfer Vehicles*, Vol. 96, Progress in Astronautics and Aeronautics, AIAA, New York, 1984.

[18]Anderson, J. D., Jr., *Hypersonic and High Temperature Gas Dynamics,* McGraw-Hill, New York, 1989.

[19]Hartung, L. C., and Hassan H. A., "Radiation Transport around Axisymmetric Blunt Body Vehicles Using a Modified Differential Approach," AIAA Paper 92-0119, 1992.

[20]Mitcheltree, R., and Gnoffo, P., "Thermochemical Nonequilibrium Issues for Earth Reentry of Mars Mission Vehicles," AIAA Paper 90-1698, 1990.

[21]Candler G. V., and MacCormack, R. W., "The Computation of Hypersonic Ionized Flows in Chemical and Thermal Nonequilibrium," AIAA Paper 88-0511, 1988.

[22]Wada, Y., Kubota, H., Ogawa, S, and Ishiguro, T., "A Generalized Roe's Approximate Riemann Solver for Chemically Reacting Flows," AIAA Paper 89-0202, 1989.

[23]Candler, G., and Park, C., "The Computation of Radiation from Nonequilibrium Hypersonic Flows," AIAA Paper 88-2678, 1988.

[24]Park, C., "On Convergence of Computation of Chemically Reacting Flows," AIAA Paper 85-0247, 1985.

[25]Elbert, G. J., and Cinnella, P., "Axisymmetric Radiative Heat Transfer Calculations for Flows in Chemical Non-equilibrium," AIAA Paper 93-0139, 1993.

[26]Elbert, G. J., "Two Dimensional and Axisymmetric Radiative Heat Transfer for Hypersonic Flow in Chemical Nonequilibrium," Ph.D. Dissertation, Mississippi State Univ., 1992.

[27]Walters, R. W., and Thomas, J. L., "Advances in Upwind Relaxation Methods," *State-of-the-Art Surveys on Computational Mechanics,* edited by A. K. Noor, ASME Publications, 1988.

[28]Grossman, B., and Cinnella, P., "Flux-Split Algorithms for Flows with Non-equilibrium Chemistry and Vibrational Relaxation," *Journal of Computational Physics,* Vol. 88, No. 1, 1990.

[29]Hankey, W. L., *Re-entry Aerodynamics,* AIAA Education Series, 1988.

[30]Cinnella, P., and Elbert, G. J., "Two-Dimensional Radiative Heat Transfer Calculations for Flows in Thermo-chemical Non-equilibrium," AIAA Paper 92-0121, 1992.

[31]Viegas, J. R., and Howe, J. T., "Thermodynamic and Transport Property Correlation Formulas for Equilibrium Air," NASA TN D-1429, 1962.